Supplemental Information for

Quantification and physical analysis of nanoparticle emissions from a marine engine using different fuels and a laboratory wet scrubber

1

Luis F. E. d. Santos,*,† Kent Salo,‡ and Erik S. Thomson*,†

†*Department of Chemistry and Molecular Biology, Atmospheric Science, University of Gothenburg, Gothenburg, Sweden*

‡*Department of Mechanics and Maritime Sciences, Maritime Studies, Chalmers University of Technology, Gothenburg, Sweden*

E-mail: luis.santos@cmb.gu.se; erik.thomson@gu.se
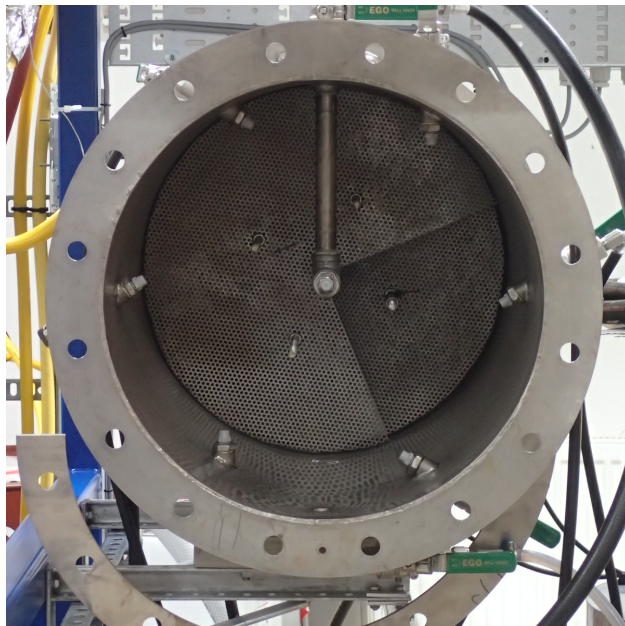
2 Laboratory Wet Scrubber (WS)

Figure S1: Internal view of the Chalmers laboratory WS with the photograph taken in the direction of exhaust flow and the inlet lid removed. The internal water nozzles (6 concentrically mounted around the interior circumference and one centrally mounted) and the rear demister plates are seen.

Aerodynamic Aerosol Classifier (AAC) Uncertainties

The sequence of instruments within the tandem Electrostatic Classifier (EC) – Aerodynamic Aerosol Classifier (AAC) set-up was reversed compared to Tavakoli and Olfert[1]. In order to avoid potential issues with multiply charged particles within the SMPS system and due to the EC 3080N having a limited upper size range (≈ 200 nm), it was decided to size select with the 3080N and to scan with the AAC. Both sequences of the tandem set-up were tested in the laboratory using well studied species, and shown to conform.

Laboratory tests were performed to determine the effective densities (ρ_{eff}) of polystyrene latex beads (PSL), sodium chloride (NaCl) and ammonium sulfate (AS; $(NH_4)_2SO_4$) particles generated from aqueous suspensions/solutions using a constant output atomizer (Model 3076, TSI Inc., USA), an electrostatic classifier EC 3080L (TSI Inc., USA) and an AAC (Cambustion Ltd., UK). Both orderings of the 3080L and the AAC were used to size select and scan the test particles. The results are compared and presented in Figure S2.

The relationship between aerodynamic (d_{ae}) and mobility diameter (d_{mo}) for spherical particles is,

$$d_{ae} = d_{\text{mo}}\sqrt{\frac{\rho_{\text{eff}}}{\rho_0}\frac{C_c(d_{\text{mo}})}{C_c(d_{ae})}}, \tag{1}$$

where ρ_0 equals a density of 1 g cm^{-3} and C_c is the Cunningham slip correction factor (cf. Eq. (4) from main text reordered).[2] Measured values are also compared to theoretical values of ρ_{eff} (Figure S2). PSL spheres are assumed to be spherical with $\rho_{\text{eff,PSL}} = 1.05$ g cm^{-3}. Similarly, AS particles are assumed to be spherical with $\rho_{\text{eff,AS}} = 1.77$ g cm^{-3}. For NaCl particles a dynamic shape factor of 1.08 (value for cubic particles[3]) was considered resulting in $\rho_{\text{eff,NaCl}} \approx 2.009$ g cm^{-3}. Size dependent deviations between the measured and theoretical ρ_{eff} were quantified and used to determine the uncertainty envelope for the effective densities of the exhaust particles. Deviations and uncertainties were only considered for particles with $d_{\text{mo}} \geq 50$ nm.

For PSL spheres, $d_{\text{mo}} \geq 100$ nm, Johnson et al.[4] observed a positive d_{mo} bias when

²⁸ using an AAC with a recently developed continuous scanning mode. Their d_{mo} bias agrees

²⁹ well with the bias we observe in ρ_{eff}, leading us to the conclusion that this represents the

³⁰ limitations of the instrument, and therefore the underlying uncertainty in the measurement
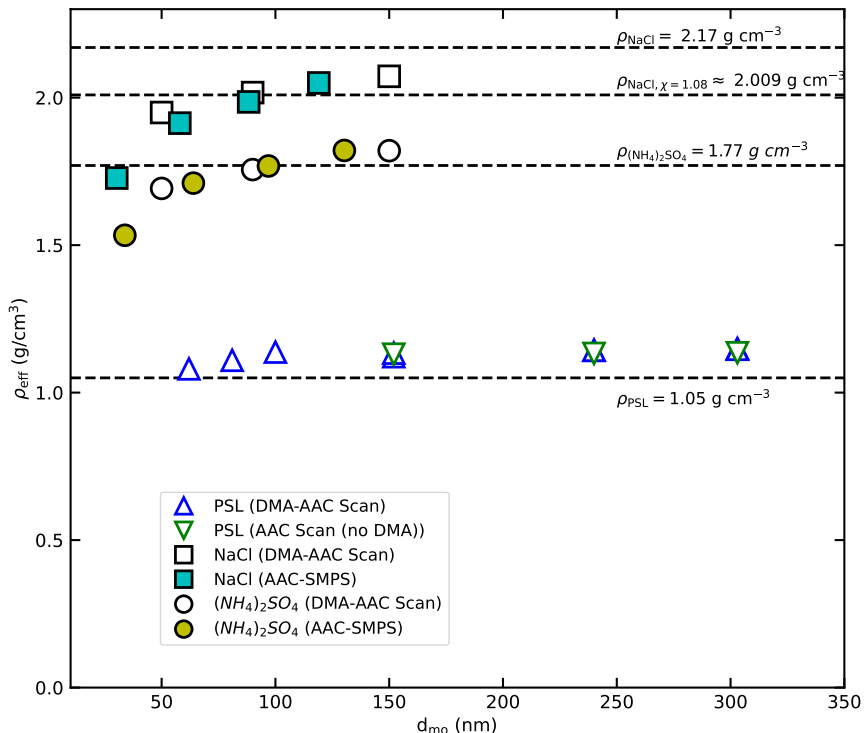
³¹ method.

Figure S2: The effective density of PSL spheres (triangles), and NaCl (squares) and AS (circles) particles measured using an EC 3080L DMA and AAC in series. Data coloring, as presented in the legend, corresponds to the DMA-AAC versus AAC-DMA instrument ordering. Dashed lines represent theoretical density values of the three compounds.

Gas Concentrations and Exhaust Temperatures

Table S1: Average gas concentrations and exhaust gas temperatures for each experimental case. Uncertainties are given as two standard deviations.

| Case	CO_2 (%)	O_2 (%)	SO_2 (ppm)	NO_x (ppm)	CO (ppm)	T_{exh} (°C)
HGO_l	7.53 ± 0.13	9.89 ± 0.16	130 ± 3	604 ± 39	521 ± 31	231.2 ± 12.3
HGO_h	7.76 ± 0.1	9.48 ± 0.19	104 ± 21	556 ± 23	431 ± 25	238.5 ± 4.9
MGO	7.77 ± 0.09	9.26 ± 0.08	0	588 ± 26	418 ± 17	238.7 ± 11.5
HVO	7.53 ± 0.09	10.22 ± 0.12	0	683 ± 19	274 ± 35	247.6 ± 11.1
FWS_l	7.47 ± 0.09	10.41 ± 0.24	22 ± 11	621 ± 18	212 ± 32	38.8 ± 1.1
FWS_h	8.05 ± 0.16	9.32 ± 0.12	22 ± 8	622 ± 31	194 ± 18	40.7 ± 0.2
SWS_l	7.12 ± 0.22	10.67 ± 0.32	0	542 ± 30	612 ± 21	42 ± 1.1
SWS_h	7.28 ± 0.09	10.41 ± 0.11	6 ± 5	554 ± 11	319 ± 13	41.5 ± 0.5

PSD - Engine Load Measurements 2021
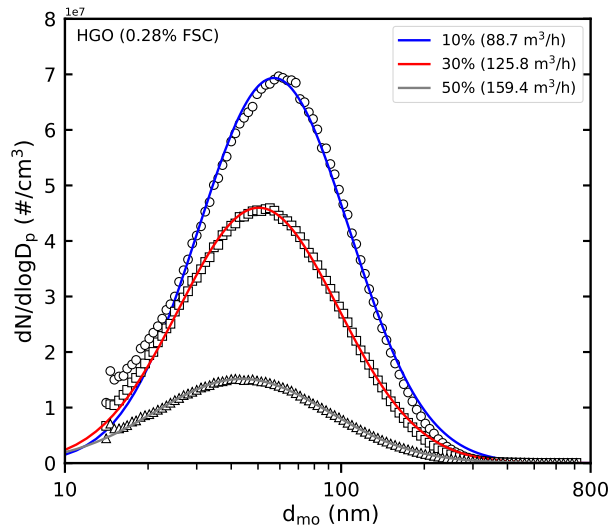
Figure S3: Particle size distributions taken from HGO exhaust using a SMPS system at 10%, 30% and 50% engine load performed in June 2021. Markers show averaged data points whereas corresponding lognormal fits are depicted by solid lines. The FSC of the fuel was 0.28%
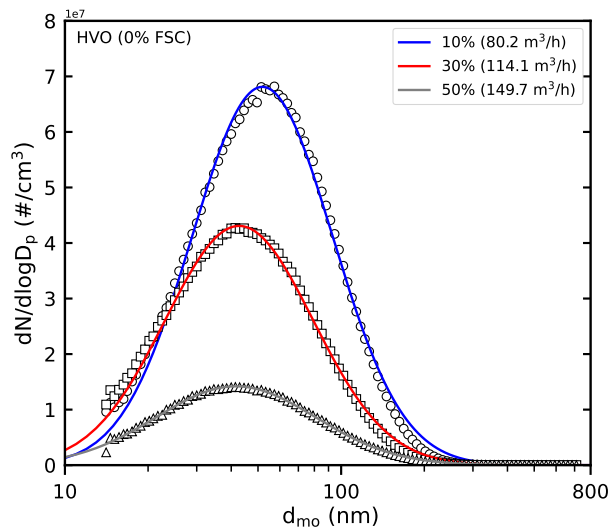

Figure S4: Particle size distributions taken from HVO exhaust using a SMPS system at 10%, 30% and 50% engine load performed in June 2021. Markers show averaged data points whereas corresponding lognormal fits are depicted by solid lines.
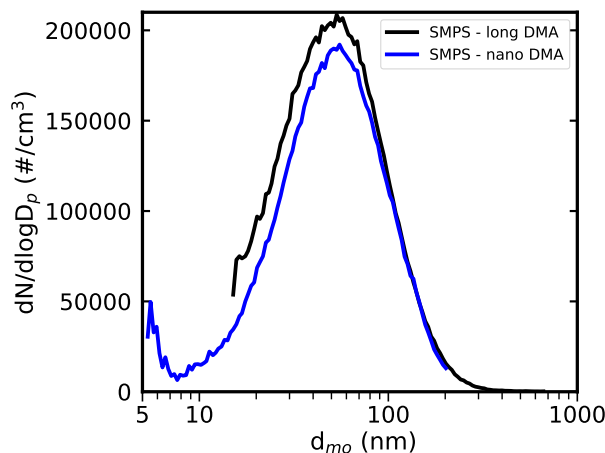
34 SMPS Comparison

Figure S5: Particle size distributions taken from HGO exhaust using SMPS systems with a long DMA (black; 15.1 nm $\leq d_{\mathrm{mo}} \leq$ 661.2 nm) and a nano DMA (blue; 5 nm $\leq d_{\mathrm{mo}} \leq$ 200 nm) that illustrate a potential particle mode around 5 nm.

35 Supplemental WS-SMPS Tests

36 Supplemental tests with the WS were performed during the campaigns. These tests included

37 diverting exhaust gas from HGO combustion through the WS without spraying water through

38 the nozzles (Figure S6). The PSDs resulting from the former tests show that the WS itself

39 does not affect the PSD substantially (Figure S6). The PSD still exhibits a unimodal size

40 distribution with a mode around 50 nm, which agrees with the control HGO experiments.

41 The peak particle concentration decreases, which is attributed to losses within the scrubber

42 system.

43   In June 2021 measurements using the same experimental set-up were performed. The

44 engine was run at 10%, 30% and 50% engine load using the same HVO batch and a new

45 HGO batch with an FSC of 0.28%. Leftover of the 0.86% HGO batch was used to increase

46 the FSC of the new batch at later stages of the experiment. Figure S7 shows a comparison

47 of HGO-WS PSDs between 2020 and 2021. In 2021 no formation of a particle mode around
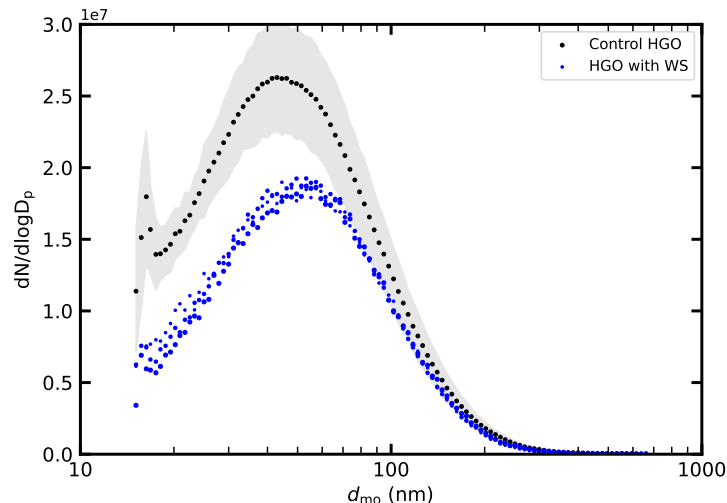
Figure S6: Comparison between a control HGO experiment (black dots) without a WS, and PSDs resulting from passing the same exhaust gas through the WS without injecting water (blue dots). A slight decrease in magnitude is observed, likely due to increased particle losses within the expanded system. The shaded area represents two standard deviations.

20 nm was observed at engine loads of 30%. When increasing the engine load to 50% and thus, also increasing the SO_2 emissions, a primary mode around 20 nm begins to develop. Different SO_2 concentrations for the 2021 examples, shown in the legend, result from the addition of the 2020 HGO batch in order to increase the FSC. No formation of primary mode particle post-WS has been observed at any engine load when HVO was used in conjunction with the WS, as shown in Figure S8. We therefore proceed with the assumption that the formation of primary mode particles is caused by the emission of gaseous sulfur containing compounds.

The system was also tested with the operational WS but without exhaust, using both a high volume blower and a hot air gun (Figure S9) to check whether water spraying in the scrubber leads to droplets that are falsely classified as particles formed from exhaust-water interactions. Results are shown in Figure S9. When using heated air from the hot gun, particle number concentrations are initially higher than in tests that use room temperature air. However, the particle number concentrations from the heated air decrease with subsequent scans until they stabilize at values similar to those observed for room temperature scans. We
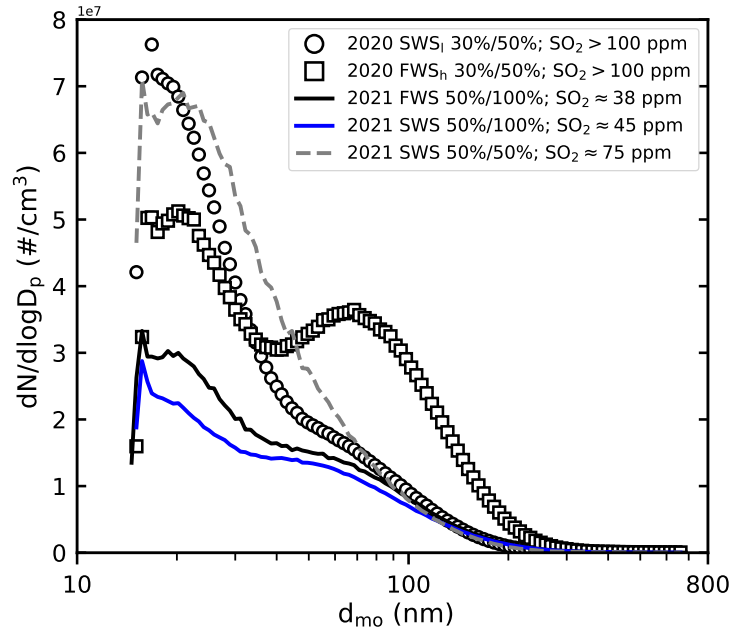
Figure S7: Comparison between SWS_l and FWS_h PSDs, represented by circles and squares respectively, and data obtained from using HGO (2021 batch) with the WS at 50% load. Percentages indicate engine load/fraction of the exhaust gas diverted through the WS.
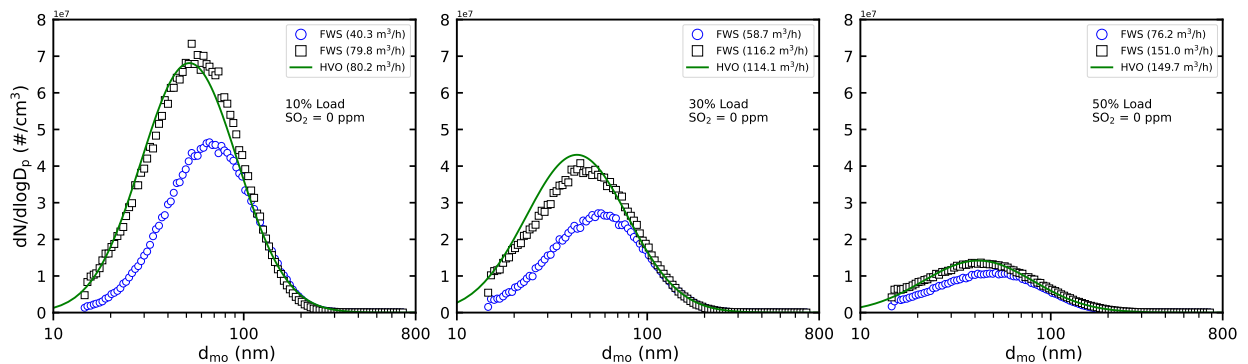

Figure S8: Measured average PSDs for HVO in conjunction with the WS at different engine loads. Blue circles show data with 50% of the exhaust gas going through the WS, black squares represent 100% of the exhaust gas going through the WS and the green solid lines show the PSDs for HVO without the WS system.

hypothesize that the initial higher concentrations are due to residues of volatile material in the system. The high air temperature causes substances to evaporate and form secondary particles in the scrubber, but with increasing time the volatile material is depleted leading the observations to stabilize. It is noteworthy that even the peak particle number concentration remains four orders of magnitude less than those resulting from the combustion of the fuels and wet scrubber experiments presented in this study. We therefore conclude that the WS itself is not a significant source of particulate and that volatile compounds within the exhaust gas can lead to secondary particle formation when exposed to wet scrubbing treatment.
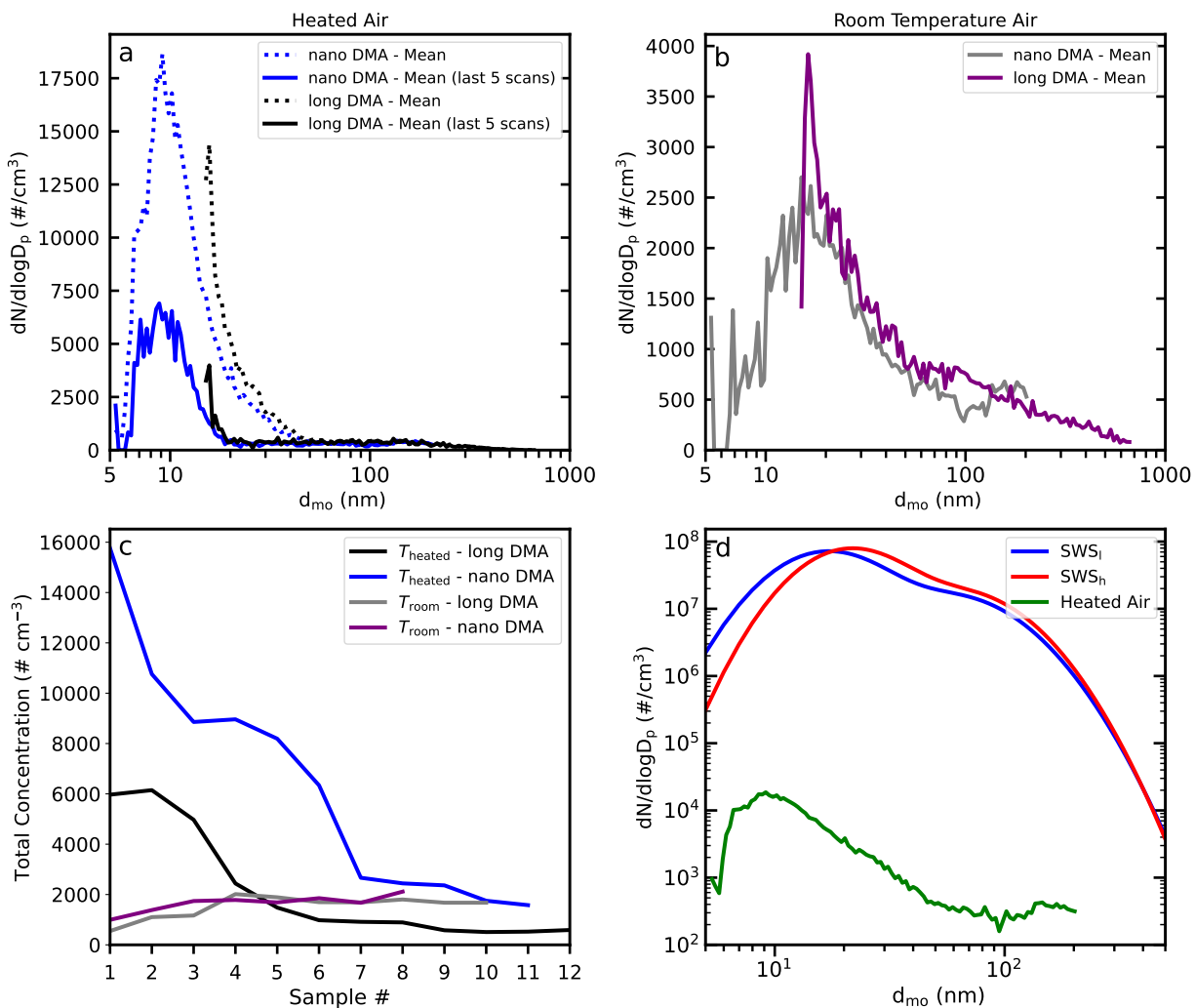
Figure S9: Measured average PSDs using long and nano DMA/SMPS systems (TSI Inc., USA). Engine exhaust was replaced with (a) air from a hot air gun and (b) room temperature air from a high volume pump. Both tests utilized the seawater scrubber. Integrated total number concentrations as a function of scan number are shown in panel c. (d) Measured average PSDs for SWS (both cases) are compared to the average PSD resulting from 5 scans when heated ambient air was coupled to the WS without engine exhaust.

Thermodenuder Plot

A systematic evaluation of PSDs using a thermodenuder (Dekati Ltd., Finland) was attempted but not completed due to instrumental issues, mainly attributed to flow parameters and leakage. However, a limited number of SWS scans are shown in Figure S10. Qualitative observations such as a strong reduction in the primary mode can be observed, although a quantitative analysis could not performed as it was difficult to determine to which degree some scans were affected by leakage. As a result, the change in the svolatile fraction of particulate due to wet scrubbing was not possible to be calculated. It should also be stated that the thermodenuder was operated using a total flow rate of 0.6 lpm, which does not meet the manufacturers recommended minimum flow rate of 10 lpm. Nevertheless, the denuded PSD was corrected according the manufacturer's correction functions.[5]
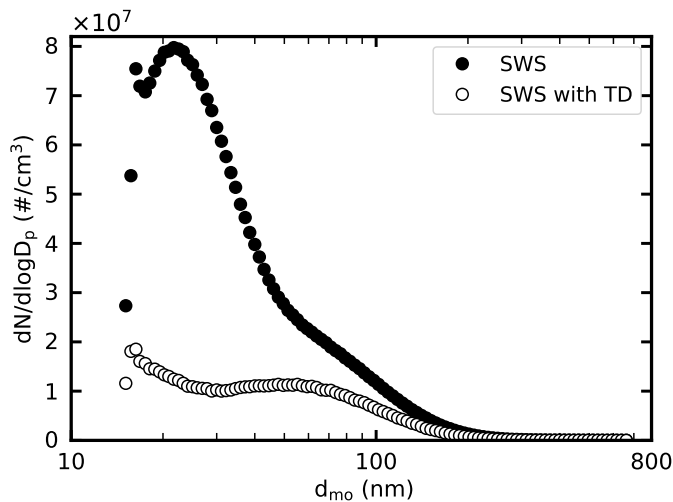

Figure S10: PSDs for SWS with and without thermodenuder (TD).

References

(1) Tavakoli, F.; Olfert, J. S. Determination of particle mass, effective density, mass-mobility exponent, and dynamic shape factor using an aerodynamic aerosol classifier and a differential mobility analyzer in tandem. *Journal of Aerosol Science* **2014**, *75*, 35–42.

(2) McMurry, P. H.; Wang, X.; Park, K.; Ehara, K. The relationship between mass and mobility for atmospheric particles: A new technique for measuring particle density. *Aerosol Science and Technology* **2002**, *36*, 227–238.

(3) Hinds, W. C. *Aerosol Technology: Properties, Behavior, and Measurement of Airborne Particles*, 2nd ed.; Wiley: New York, 1999.

(4) Johnson, T. J.; Symonds, J. P.; Olfert, J. S.; Boies, A. M. Accelerated measurements of aerosol size distributions by continuously scanning the aerodynamic aerosol classifier. *Aerosol Science and Technology* **2021**, *55*, 119–141.

(5) Dekati Ltd., Thermodenuder User Manual. 2003.